Observation of Square-Root Higher-Order Topological States in Photonic Waveguide Arrays

Juan Kang[a], Tao Liu[b,a], Mou Yan[b], Dandan Yang[a], Xiongjian Huang[a], Ruishan Wei[a], Jianrong Qiu[c], Guoping Dong[a,*], Zhongmin Yang[b,*], Franco Nori[d]

[a]*State Key Laboratory of Luminescent Materials and Devices, and Guangdong Provincial Key Laboratory of Fiber Laser Materials and Applied Techniques, Guangdong Engineering Technology Research and Development Center of Special Optical Fiber Materials and Devices, School of Materials Science and Engineering, South China University of Technology, Guangzhou 510640, China*

[b]*School of Physics and Optoelectronics, South China University of Technology, Guangzhou 510640, China*

[c]*State Key Laboratory of Modern Optical Instrumentation, College of Optical Science and Engineering, Zhejiang University, Hangzhou 310027, China*

[d]*Theoretical Quantum Physics Laboratory, RIKEN Cluster for Pioneering Research; RIKEN Center for Quantum Computing (RQC), Wako-shi, Saitama 351-0198, Japan; and Department of Physics, University of Michigan, Ann Arbor, Michigan 48109-1040, USA*

* To whom correspondence should be addressed.

E-mail: dgp@scut.edu.cn (G.P. Dong); yangzm@scut.edu.cn (Z.M. Yang)

Recently, higher-order topological insulators (HOTIs), accompanied by topologically nontrivial boundary states with codimension larger than one, have been extensively explored because of unconventional bulk-boundary correspondences. As a novel type of HOTIs, very recent works have explored the square-root HOTIs,

This is the author manuscript accepted for publication and has undergone full peer review but has not been through the copyediting, typesetting, pagination and proofreading process, which may lead to differences between this version and the Version of Record. Please cite this article as doi: 10.1002/lpor.202200499.

where the topologically nontrivial nature of bulk bands stems from the square of the Hamiltonian. In this paper, we experimentally demonstrate 2D square-root HOTIs in photonic waveguide arrays written in glass using femtosecond laser direct-write techniques. Edge and corner states are clearly observed at visible light spectra. The dynamical evolutions of topological boundary states are experimentally demonstrated, which verify the existence of photonic corner states in two band gaps. The symmetry-protected corner states in the photonic square-root HOTI may have potential applications in information processing and lasing.

1. Introduction

Topological insulators (TIs) have attracted intense research interests due to their exotic electronic and optical properties as well as promising device applications[1-3]. Recently, the concept of TIs has been generalized to higher-order topological insulators (HOTIs). In contrast to first-order TIs, *n*th-order HOTIs[4-8] feature gapless states on their open boundaries with codimension *n*. For instance, a two-dimensional (2D) HOTI hosts mid-gap states on its 0D corners. The higher-order topological phases have been widely investigated in both condensed matter physics[9-11] and classical waves systems, such as photonic crystals[12-20], acoustic systems[21-23], and mechanical systems[24,25]. Noticeably, for photonic systems, higher-order topological states can find novel applications in, e.g., achieving 0D low-threshold and high-performance topological lasing in 2D photonic crystals[26-30], and designing topological photonic crystal fibers with multi-channel transmission capabilities based on corner modes[14,15].

Recently, a novel type of TIs has been put forward by taking the square root of tight-binding models, dubbed square-root Tis[31]. Their Hamiltonians are obtained by applying the square-root operation to their parent Hamiltonians, thus giving rise to doubled bulk gaps. The square-root TIs can support boundary states with non-quantized topological indices, as demonstrated in 1D chains of Aharonov-Bohm cages[32]. Later on, the square-root topology has been extended to other systems including superconductors and non-Hermitian structures[33]. Specially, the square-root operation was generalized to HOTIs, producing square-root HOTIs[34]. The square-root HOTIs can be obtained by inserting a set of additional sublattices in an original lattice, and the topological properties are inherited from their squared Hamiltonians. The corresponding experimental realization was actively pursued in various classical wave systems, such as acoustic and electromagnetic waves[35,36]. In contrast to conventional HOTIs (e.g., the kagome and honeycomb lattices[14,15]) with one group of corner/edge states, the square-root HOTIs host two groups of corner/edge states in two band gaps. The two groups of corner states are localized on the two nearest sites at the corners, exhibiting opposite phase distributions. These unique properties can be further transferred into photonics, and may provide new approaches for light guiding and trapping.

Here, we experimentally realize a 2D square-root HOTI in photonic waveguide arrays written in fused quartz glass by femtosecond (fs) laser direct-write technology[37-44]. The square-root HOTI is constructed by inserting breathing kagome lattices into the honeycomb lattices[34], where corner states exist in the two band gaps. In ref.[45], the authors constructed the same square-root HOTI with its topology characterized by the bulk polarization, and reported the spectral measurements of corner localized in-gap modes. In contrast, in addition to the spectral measurement,

we analyze a fractional corner anomaly for revealing the higher-order topology, and explored the confinement and dynamical features of visible-light excitation on the lattice boundaries. Furthermore, the robustness of the corner states against disorder respecting the corresponding symmetry is discussed, which is of significance for the practical applications.

2. Results

2.1. Model

The square-root HOTI is designed by a combination of a honeycomb lattice and a breathing kagome lattice[34]. This forms a decorated honeycomb lattice, as shown in **Figure 1**a. The Hamiltonian of the combined system is derived by applying the square root operator to the direct sum of two Hamiltonians of the honeycomb and breathing kagome lattices. The photonic square-root HOTI can be realized in optical waveguide arrays via fs laser direct-write. In the single-mode approximation, the waveguide arrays can be described by using a tight-binding approximation. The diffraction equation of the light propagation along this structure reads:

$$i\partial_z \psi(z,\lambda) = H(\lambda)\psi(z,\lambda), \tag{1}$$

where $\psi(z,\lambda)$ denotes the envelope of the electric field in the waveguide with propagation distance z, and λ is the wavelength of light. The effective tight-binding Hamiltonian for the decorated honeycomb lattice is given by

$$H^2 = \begin{pmatrix} H_p^{(H)} & 0 \\ 0 & H_p^{(K)} \end{pmatrix}, \tag{2}$$

where $H_p^{(K)}$ represents the Hamiltonian of the breathing kagome lattices, and $H_p^{(H)}$ represents the Hamiltonian of honeycomb lattices with on-site potentials of two sublattices. $H_p^{(H)} = hh^{\dagger}$, and $H_p^{(K)} = h^{\dagger}h$, with

$$h = \begin{pmatrix} c_1 & c_1 & c_1 \\ c_2 & c_2 e^{i\boldsymbol{k}\boldsymbol{a_1}} & c_2 e^{i\boldsymbol{k}\boldsymbol{a_2}} \end{pmatrix}, \quad (3)$$

where $\boldsymbol{k}$ denotes Bloch wavevector, $\boldsymbol{a}_{1,2}=(\pm 1/2, \sqrt{3}/2)$ are the lattice vectors, c_1 and c_2 are coupling coefficients between nearest-neighbor waveguides, which depend on the wavelength λ and the distance d of the adjacent waveguides. The topological properties of the decorated honeycomb lattice are described by its squared Hamiltonian, which includes two sectors $H_p^{(H)}$ and $H_p^{(K)}$. Here, we consider the bulk polarization as a topological invariant[22,34]. For our square-root system with C_3 symmetry, the quantized polarization below the first and second gaps are P=1/3 for $c_1 > c_2$, respectively, indicating a topologically nontrivial phase. While for $c_1 < c_2$, a topologically trivial phase occurs with zero polarization P=0. Note that the polarizations for the eigenvector of the kagome sector $H_p^{(K)}$ has the same variation as P. Whereas the polarizations for the eigenvector of the honeycomb sector $H_p^{(H)}$ is always 0 for $c_1 > c_2$ and $c_1 < c_2$. This indicates that the nontrivial topological properties of the square-root HOTI are inherited from the inserted kagome lattice.

The schematic of the decorated honeycomb lattice in the photonic waveguide array is shown in **Figure 1**b. The diameter of each waveguide is 8.5 μm, and the refractive index difference between the waveguide and glass matrix is estimated to be 3.3×10^{-4}, corresponding to the propagation constant $\beta_0 = 17.23$ μm^{-1} at $\lambda =$ 532 nm. For the waveguide system in the topologically nontrivial regime, the two characteristic distances between nearest-neighbor waveguides are d_1=12 μm, and

$d_2 = 21$ μm (corresponding to c_1=2.66 cm^{-1}, and c_2=0.36 cm^{-1}). And the system becomes topologically trivial once d_1 is interchanged with d_2.

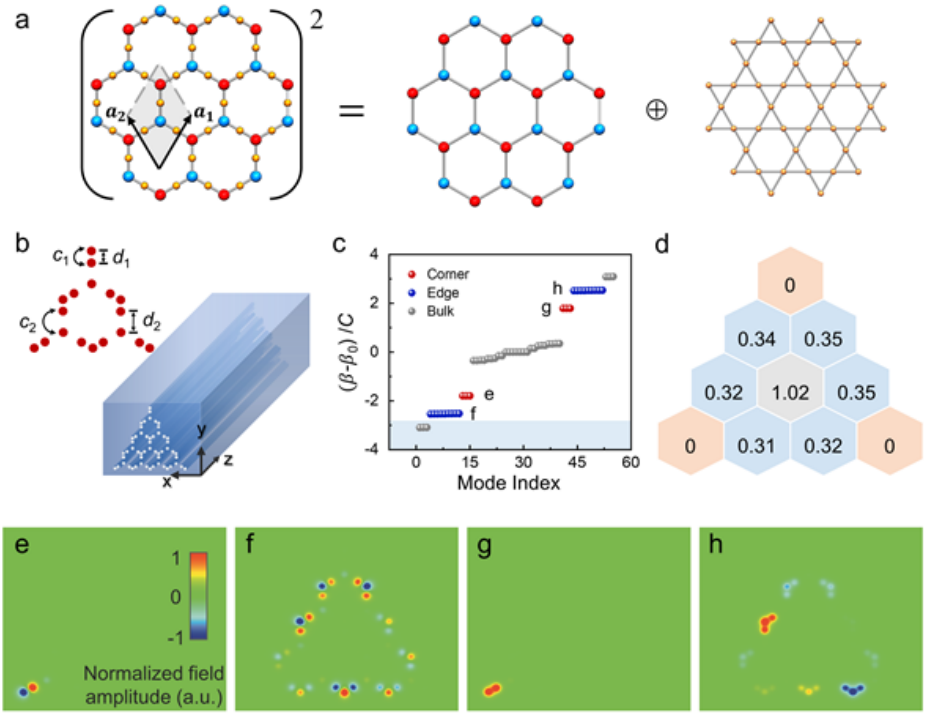

Figure 1. Structure and spectrum of the finite decorated honeycomb lattice. a) The square of the Hamiltonian of the decorated honeycomb lattice is the direct sum of the Hamiltonians of honeycomb and breathing kagome lattices. Black arrows represent the lattice vectors: $a_{1,2}=\left(\pm\frac{1}{2},\frac{\sqrt{3}}{2}\right)$. b) Schematic showing the optical waveguide array with the decorated honeycomb lattice. The lattice constant a=33 μm, c_1 and c_2 denote the coupling strengths defined in Eq. (3), d_1=12 μm and d_2=21 μm. c) Calculated eigenspectra of the finite lattice with the corner (red), edge (blue) and bulk (gray) states. $C=(c_1+c_2)/2$=1.51 cm^{-1}. d) Distribution of the photonic charge for the first bulk band (marked by the blue shadow in (c)). e,g) Simulated mode field distributions of corner states in the first and second band gaps. f,h) Simulated mode field distributions of edge states in the first and second band gaps.

Figure 1c shows the simulated eigenspectra of the finite photonic lattice in the topologically nontrivial regime, where the corner and edge states emerge in two band gaps. We then calculate the distribution of the photonic charge by integrating the local density of states over the first band, as shown in **Figure 1**d (more details are shown in Section S2, Supporting Information). A fractional charge $\sigma_{edge} \approx 1/3$ appears at the edge, and vanishes at the corner with $\sigma_{corner} \approx 0$. Thus, a fractional corner anomaly $Q = \sigma_{corner} - (\sigma_{edge1} + \sigma_{edge2}) \bmod 1 \approx 1/3$ occurs, indicating the existence of higher-order topological corner states[46-48].

The mode profiles of the corner and edge states in the two band gaps are shown in **Figures 1**e-h. This square root HOTI is strikingly different from the conventional second-order kagome lattice. For the kagome lattice, the topologically nontrivial phase corresponds to the weak intercell coupling, and its second-order topological corner states are well localized at a single isolated site at each corner[14,49]. While, for our decorated honeycomb lattice, the strong intercell coupling leads to a series of coupled “triplets” (three excited sites) along the edges and “duplets” (two excited sites) on each corner. Moreover, these boundary states in the first and second band gaps show the antiphase and in-phase mode profiles.

2.2. Observation of boundary states

We now proceed to experimentally probe the in-gap edge and corner states to demonstrate features of the photonic square-root HOTI. We fabricate the decorated honeycomb lattice in optical waveguide arrays as shown in **Figure 2**a. A laser beam with a wavelength of 532 nm is injected into the corner/edge waveguides through the fused-tapered optical fiber. Light localization, in the coupled duplets waveguides of the corner (or the triplet waveguides of the edges), is observed, as presented in **Figures 2**b,c. For comparison, we fabricate two additional samples with homogeneous (**Figure 2**d) and trivial (**Figure 2**g) configurations, corresponding to

d_1=d_2=16.5 μm, and d_1=21 μm, d_2=12 μm, respectively. In the homogeneous lattice, the light injected into the corner and edge waveguides diffracts into the bulk (see **Figures 2**e,f), due to the bulk band-gap closure. For the trivial case, there are no corner/edge states although the band gaps reopen, light spreading also occurs (see **Figures 2**b,c). The corresponding numerical simulations are presented in **Figure S3**, Supporting Information, which confirm our experimental results. In addition, the experimental results about bulk and defect states are shown in Section S4, Supporting Information. The same topological features can be detected using other excitation wavelengths, by simply modifying the waveguide spacing. In **Figure S8**, we present the localized corner and edge states under the excitations of both blue and red light.

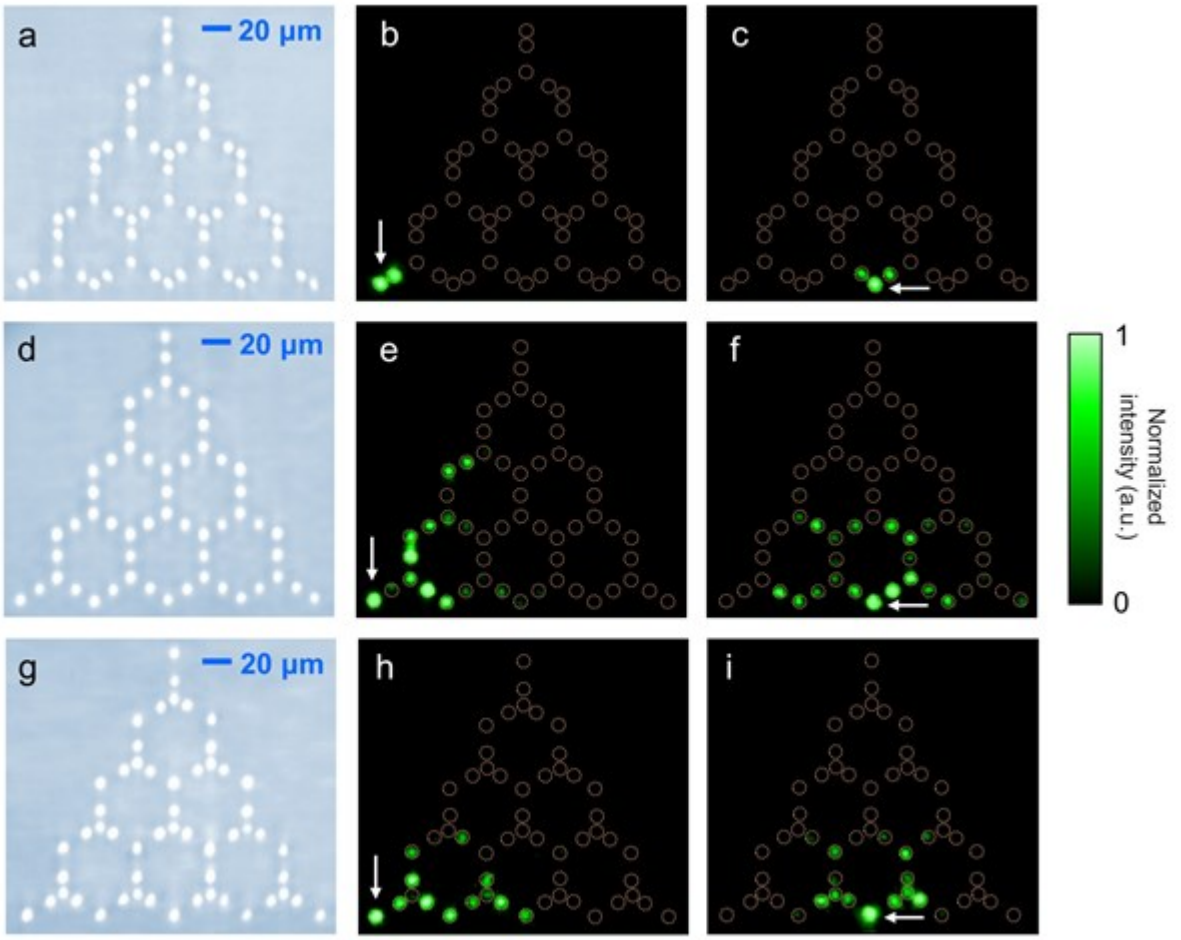

Figure 2. Experimental observation of corner and edge states. a), d) and g): Microscope images of the waveguide arrays for the topologically nontrivial, homogeneous and trivial photonic lattices, respectively. b, c) Experimental images of light emerging at the output facet of the samples in (a) by injecting light (λ=532 nm) into the corner and edge waveguides (marked by a white arrow), respectively. The light is localized at a corner and edge. e,f) and h,i): same as b,c) but for the homogeneous and topologically trivial cases, where light is diffracted into the bulk. The dashed circles denote the positions of the waveguides. All of the samples have the same length z=49 mm.

2.3. Dynamical evolutions

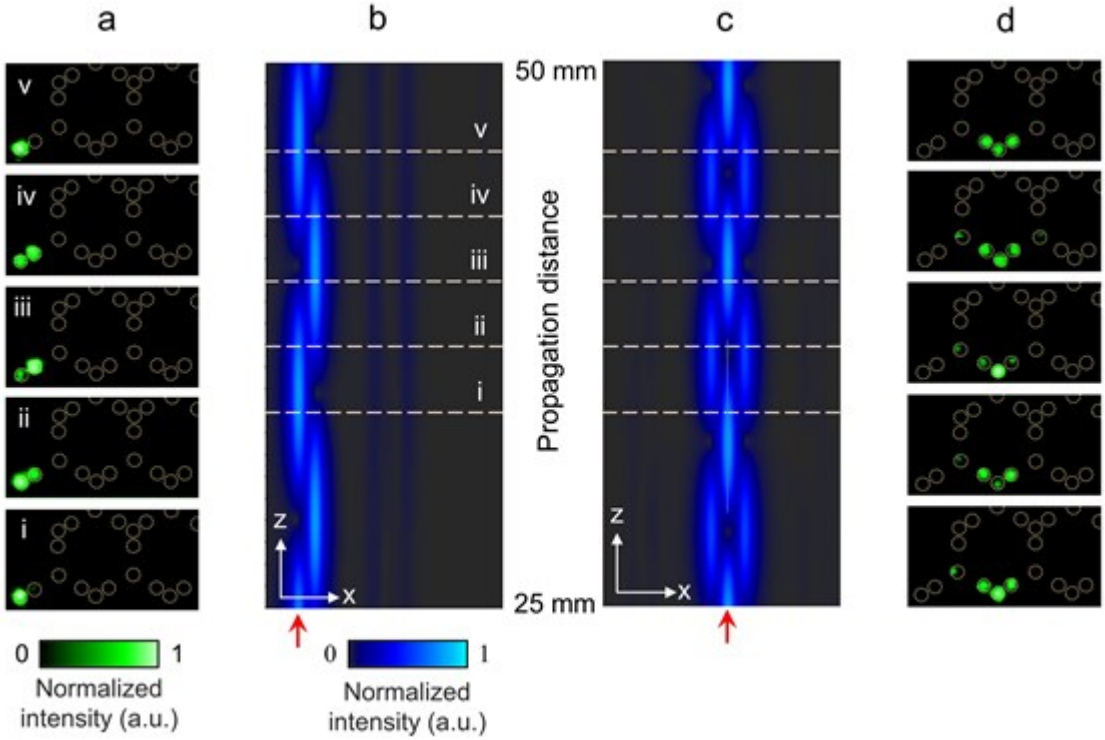

Figure 3. Dynamical evolutions of the corner and edge states. a) Measured distributions of light at the output facet of samples with different lengths. i-v denote waveguides with lengths *z*=34, 37, 40, 43, 46 mm, respectively. b) Simulated propagation dynamics of light when exciting the first waveguides at the left corner. C) Simulated light propagation dynamics, and d measured light distributions when exciting the first waveguides at the edge. Red arrows indicate the positions of the excited waveguides. Note that only parts of the simulation results (propagation distance from 25 mm to 50 mm) are displayed in (b) and (c).

Topological properties of the square-root HOTIs are further explored by studying the propagating dynamics, along the z-direction, of the boundary states. The evolution time t of the wavefunction in tight-binding models can be mapped into the propagation distance z of light in optical waveguide arrays. We fabricated five

samples with different lengths (**Figure 3**), and probed the light distributions at the output facet. Upon exciting the first (**Figures 3**a,b) or the second waveguide (**Figure S9**, Supporting Information) at the left corner, the light propagates alternately in the two waveguides at the corner along the z-direction. When exciting the waveguide on the edge (**Figures 3**c,d), a breathing-like oscillation is observed in the triplet waveguides. These experimental observations are consistent with numerical simulations using the beam-propagation method. In particular, when injecting light into the waveguides at the corner, both topologically protected corner states with the antiphase and in-phase distributions are excited simultaneously. Thus, the two corner states with different eigenenergies are superimposed, resulting in the light-beating phenomenon. The energy difference of these two corner states is derived as $\Delta\beta = \pi/l$, with $l = 0.57$ cm being the beating length. Therefore, we obtain the energy of the corner states as $\beta_c = \beta_0 \pm 2.75$ cm^{-1}, in agreement with the numerical results in **Figure 1**c. The beating pattern reveals the existence of corner states in two band gaps in the photonic square-root HOTI.

2.4. Robustness of the higher-order corner states

The higher-order in-gap corner states are expected to be robust against disorder preserving the C_3 symmetry which enforces the quantized bulk polarization. To demonstrate this, we introduce disorder by randomly changing the nearest-neighbor coupling, sampled as a uniform distribution in the range $[-W/2, W/2]$. The disorder strength is defined as $\delta=\sigma/C$, where $\sigma=W/\sqrt{12}$ is the standard deviation of uniformly distributed random numbers (see details in Section S7, Supporting Information).

We consider two types of disorder, which preserve and break the C_3 symmetry, respectively. For the former case, we find that the C_3-preserving disorder only induces a slight fluctuation of the energies (denoted by the propagation constant) of the corner states for small disorder strength (see **Figure 4**a). Moreover, The inverse participation ratio (IPR) is independent of system length, because second-order topological boundary states are always localized around the corners. (see **Figure 4**b). These results indicate that the corner states are robust against the C_3-preserving disorder[32]. While, for the disorder strength that beyond the size of the gap between the corner state and the edge state, the energy fluctuations become stronger (see **Figure 4** and **Figure S12**b, Supporting Information). The IPR scales inversely with the system length, indicating the corner states are coupled to edge/bulk states.

In contrast, for the latter case, the energies of corner states are sensitive to the disorder, and they can coupled with the edge and bulk states in the presence of the C_3-breaking disorder, as shown in **Figure 4**a (see also **Figure S12**c, Supporting Information). In **Figure 4**c-e, we found that the light injected into the corner waveguides spreads into the bulk/edge by incrementally increasing the strength of the C_3 symmetry breaking (δ=0.10, 0.28, and 0.40). The energy fluctuations that are proportional to the disorder strength and the delocalization of the corner states indicate that there is no topological protection when the C_3 symmetry is broken. In addition, the effects of the on-site disorder on corner states are discussed in Section S7, Supporting Information, which further confirms that the corner states in the photonic square-root HOTI are protected by the C_3 symmetry.

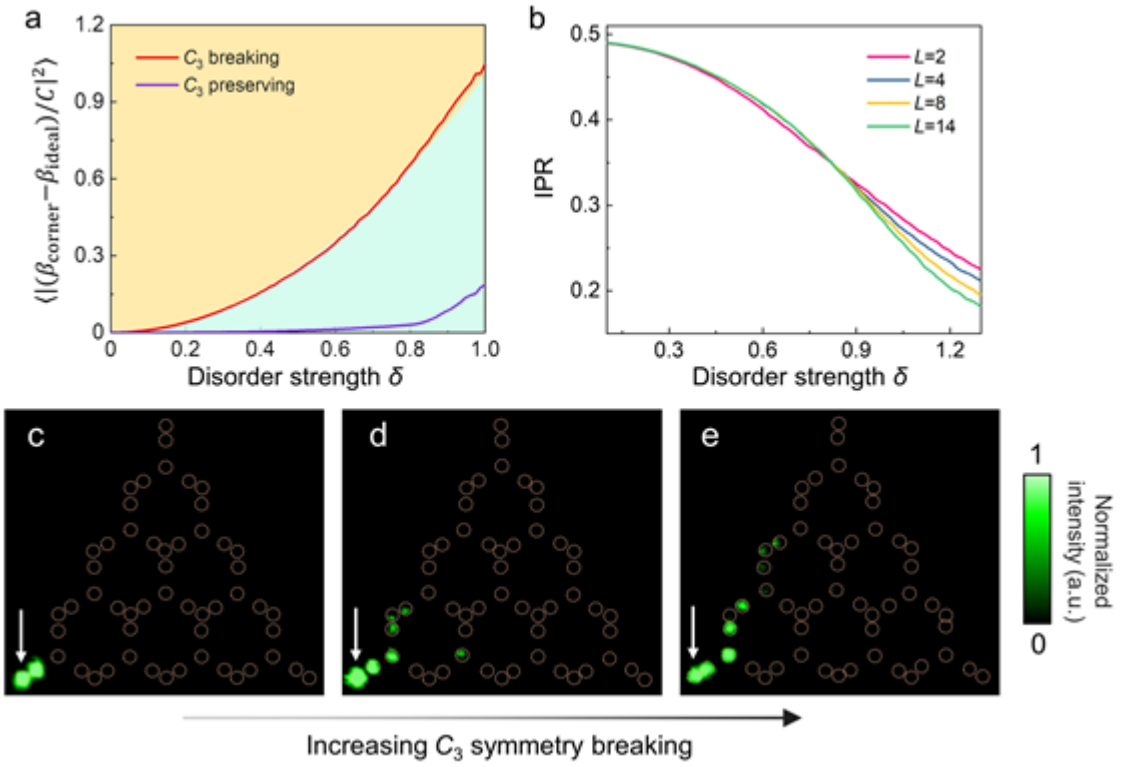

Figure 4. Robustness analysis of corner states. a) Energy fluctuations of the corner states versus disorder strength δ. The vertical axis denotes the averaged mean squared difference between the energy β_{corner} of the corner state in the disordered system and the corner-state energy β_{ideal} in the clean system. The intersected curve of the orange and cyan regions has the form δ^2 and represents the energy fluctuation proportional to the disorder strength. The simulations were run using a lattice with 342 sites and every disorder strength was realized 10,000 times. b) The inverse participation ratio (IPR) of the corner states as a function of δ for different system lengths L with the C_3-preserving disorder. Here, L is defined as the number of unit cells along the edge. c-e) Measured distributions of the light emerging at the output facet of the C_3 symmetry breaking arrays for the corner excitation, with incrementally increasing strength δ=0.10, 0.28 and 0.40.

3. Discussion

In summary, we have realized 2D photonic square-root HOTIs based on optical waveguide arrays fabricated in glass using femtosecond laser direct-write techniques. In contrast to conventional higher-order photonic crystals, the square-root HOTIs host two types of corner states with in-phase and anti-phase mode profiles in two band gaps. They induce the beating pattern, which has been experimentally demonstrated by the dynamical evolution of the light in the waveguides. These findings offer a feasible strategy for controlling symmetry-protected localized states, and pave a way toward potential applications in photonic devices. Noted that our photonic decorated honeycomb lattices have similar geometry with the 2D photonic chained lattice whose topology comes from their primary lattice nodes[50]. For our system, the nontrivial higher-order topological properties are inherited from the inserted kagome lattice.

For future studies, it is worth to further explore experimentally the interplay of square-root higher-order topology and nonlinearity (see our numerical simulations in the Supplementary Information). The most recent investigations have demonstrated fascinating topological nonlinear phenomena, such as nonlinearity-induced topological phase transitions from trivial states[51], nontrivial coupling of topological states[52], and Floquet edge solitons for unidirectional transmission [53,54]. Furthermore, the experimental studies in nonlinear HOTI systems indicated that the higher-order corner states have the potential to enhance nonlinear light−matter interactions[55]. Meanwhile, the nonlinear effect can in turn promote the localization of the corner states[56,57]. We expect that incorporating the square-root higher-order topology and nonlinearity will bring more interesting topological phenomena and potential new applications of corner modes.

4. Methods

Sample fabrication: Waveguide arrays were fabricated with 50 mm commercial quartz glasses by using fs laser processing. This system consists of a regeneratively amplified Ti: sapphire fs laser, a Nikon microscope (Eclipse 80i) equipped with a CCD camera, a computer-controlled 3D *xyz* translation stage, and several optical elements. The fs laser emits 1 kHz, 130 fs pulses with central wavelength of 800 nm. To write the waveguide arrays, laser pulses with 2.5 mW power were focused inside the sample with a 20× microscope objective (NA= 0.45). The glass sample was placed on the 3D *xyz* translation stage, and then translated at a speed of 300 μm/s. An adjustable slit, oriented parallel to the laser writing direction, is inserted in front of the objective to shape the laser beam and fabricate the near-circular cross-section waveguide (see details in Section S3, Supporting Information). The fabricated waveguides support a single-mode guide over the entire visible wavelength range. After the waveguide arrays were fabricated, the two lateral faces of the sample were carefully polished. Finally, 49 mm waveguide array samples were used for the observation of topological phenomena.

Acknowledgements

J.K. and T.L. contributed equally to this work. This work was financially supported by the Key R&D Program of Guangzhou (202007020003), National Natural Science Foundation of China (Grant Nos. 62122027, 52002128, 62075063, 51772101, 51872095), Local Innovative and Research Teams Project of Guangdong Pearl River Talents Program (2017BT01X137). T.L. acknowledges the support from the Startup Grant of South China University of Technology (Grant No. 20210012). F.N. is

supported in part by: Nippon Telegraph and Telephone Corporation (NTT) Research, the Japan Science and Technology Agency (JST) [via the Moonshot RD Grant Number JPMJMS2061], the Japan Society for the Promotion of Science (JSPS) [via the Grants-in-Aid for Scientific Research (KAKENHI) Grant No. JP20H00134], the Army Research Office (ARO) (Grant No. W911NF-18-1-0358), the Asian Office of Aerospace Research and Development (AOARD) (via Grant No. FA2386-20-1-4069), and the Foundational Questions Institute Fund (FQXi) via Grant No. FQXi-IAF19-06. The authors thank D. Tan for technical assistance and W. Chen for helpful discussions.

Conflict of Interest

The authors declare no conflict of interest.

Keywords

symmetry-protected corner states, square-root higher-order topological insulators, femtosecond laser direct-write techniques, photonic waveguide arrays

References

[1] M. Z. Hasan, and C. L. Kane, *Rev. Mod. Phys.* **2010**, 82**,** 3045.

[2] X. L. Qi, and S. C. Zhang, *Rev. Mod. Phys.* **2011**, 83**,** 1057.

[3] T. Ozawa, H. M. Price, A. Amo, N. Goldman, M. Hafezi, L. Lu, M. C. Rechtsman, D. Schuster, J. Simon, O. Zilberberg, and I. Carusotto, *Rev. Mod. Phys.* **2019**, 91, 015006.

[4] W. A. Benalcazar, B. A. Bernevig, and T. L. Hughes, *Science* **2017**, 357**,** 61.

[5] F. Schindler, A. M. Cook, M. G. Vergniory, Z. Wang, S. P. Parkin, B. A. Bernevig, and T. Neupert, *Sci. Adv.* **2018**, 4**,** eaat0346.

[6] Z. Song, Z. Fang, and C. Fang, *Phys. Rev. Lett.* **2017**, 119**,** 246402.

[7] F. K. Kunst, G. Van Miert, and E. J. Bergholtz, *Phys. Rev. B* **2018**, 97, 241405.

[8] T. Liu, J. J. He, and F. Nori, *Physical Review B* **2018**, 98, 245413.

[9] M. Ezawa, *Phys. Rev. Lett.* **2018**, 120**,** 026801.

[10] T. Liu, Y. R. Zhang, Q. Ai, Z. Gong, K. Kawabata, M. Ueda, and F. Nori, *Phys. Rev. Lett.* **2019**, 122**,** 076801.

[11] S. A. A. Ghorashi, T. Li, and T. L. Hughes, *Phys. Rev. Lett.* **2020**, 125, 266804.

[12] S. Mittal, V. V. Orre, G. Zhu, M. A. Gorlach, A. Poddubny, and M. Hafezi, *Nat. Photonics* **2019**, 13, 692.

[13] M. Li, D. Zhirihin, M. Gorlach, X. Ni, D. Filonov, A. Slobozhanyuk, A. Alù, and A. B. Khanikaev, *Nat. Photonics* **2019**, 1**4,** 89.

[14] A. El Hassan, F. K. Kunst, A. Moritz, G. Andler, E. J. Bergholtz, and M. Bourennane, *Nat. Photonics* **2019**, 13, 697.

[15] J. Noh, W. A. Benalcazar, S. Huang, M. J. Collins, K. P. Chen, T. L. Hughes, and M. C. Rechtsman, *Nat. Photonics* **2018**, 12**,** 408-415.

[16] B. Y. Xie, G. X. Su, H. F. Wang, H. Su, X. P. Shen, P. Zhan, M. H. Lu, Z. L. Wang, and Y. F. Chen, *Phys. Rev. Lett.* **2019**, 122**,** 233903.

[17] X. D. Chen, W. M. Deng, F. L. Shi, F. L. Zhao, M. Chen, and J. W. Dong, *Phys. Rev. Lett.* **2019**, 122, 233902.

[18] B. Y. Xie, H. F. Wang, H. X. Wang, X. Y. Zhu, J. H. Jiang, M. H. Lu, and Y. F. Chen, *Phys. Rev. B* **2018**, 98, 582.

[19] A. Cerjan, M. Jurgensen, W. A. Benalcazar, S. Mukherjee, and M. C. Rechtsman, *Phys. Rev. Lett.* **2020**, 125**,** 213901.

[20] D. Leykam, and D. A. Smirnova, *Nat. Phys.* **2021**, 17, 632.

[21] H. Xue, Y. Yang, F. Gao, Y. Chong, and B. Zhang, *Nat. Mater.* 2019, **18,** 108-112.

[22] X. Ni, M. Weiner, A. Alù, and A. B. Khanikaev, *Nat. Mater.* **2019**, 18, 113.

[23] X. Zhang, H. X. Wang, Z. K. Lin, Y. Tian, B. Xie, M. H. Lu, Y. F. Chen, and J. H. Jiang, *Nat. Phys.* **2019**, 15, 582.

[24] M. Serra-Garcia, V. Peri, R. Susstrunk, O. R. Bilal, T. Larsen, L. G. Villanueva, and S. D. Huber, *Nature* **2018**, 555, 342.

[25] H. Fan, B. Xia, L. Tong, S. Meng, and D. Yu, *Phys. Rev. Lett.* **2019**, 122, 204301.

[26] G. Harari, M. A. Bandres, Y. Lumer, M. C. Rechtsman, Y. D. Chong, M. Khajavikhan, D. N. Christodoulides, and M. Segev, *Science* **2018**, 359, eaar4003.

[27] M. A. Bandres, S. Wittek, G. Harari, M. Parto, J. Ren, M. Segev, D. N. Christodoulides, and M. Khajavikhan, *Science* **2018**, 359, eaar4005.

[28] W. Zhang, X. Xie, H. Hao, J. Dang, S. Xiao, S. Shi, H. Ni, Z. Niu, C. Wang, K. Jin, X. Zhang, and X. Xu, *Light Sci. Appl.* **2020**, 9, 109.

[29] H. R. Kim, M. S. Hwang, D. Smirnova, K. Y. Jeong, Y. Kivshar, and H. G. Park, *Nat. Commun.* **2020**, 11, 5758.

[30] Y. Ota, F. Liu, R. Katsumi, K. Watanabe, K. Wakabayashi, Y. Arakawa, and S. Iwamoto, *Optica* **2019**, 6, 786.

[31] J. Arkinstall, M. H. Teimourpour, L. Feng, R. El-Ganainy, and H. Schomerus, *Physical Review* B **2017**, 95, 165109.

[32] M. Kremer, I. Petrides, E. Meyer, M. Heinrich, O. Zilberberg, and A. Szameit, *Nat. Commun.* **2020**, 11**,** 907.

[33] M. Ezawa, *Phys. Rev. Research* **2020**, 2, 033397.

[34] T. Mizoguchi, Y. Kuno, and Y. Hatsugai, *Phys. Rev. A* **2020**, 102, 033527.

[35] M. Yan, X. Huang, L. Luo, J. Lu, W. Deng, and Z. Liu, *Phys. Rev. B* **2020**, 102, 180102.

[36] L. Song, H. Yang, Y. Cao, and P. Yan, *Nano. Lett.* **2020**, 20, 7566.

[37] M. C. Rechtsman, J. M. Zeuner, Y. Plotnik, Y. Lumer, D. Podolsky, F. Dreisow, S. Nolte, M. Segev, and A. Szameit, *Nature* **2013**, 496, 196.

[38] Y. Ke, X. Qin, F. Mei, H. Zhong, Y. S. Kivshar, and C. Lee, *Laser Photonics Rev.* **2016**, 10**,** 995.

[39] J. Noh, S. Huang, K. P. Chen, and M. C. Rechtsman, *Phys. Rev. Lett.* **2018**, 120, 063902.

[40] Y. Lumer, M. A. Bandres, M. Heinrich, L. J. Maczewsky, H. Herzig-Sheinfux, A. Szameit, and M. Segev, *Nat. Photonics* **2019**, 13, 339.

[41] Y. Wang, X. L. Pang, Y. H. Lu, J. Gao, Y.-J. Chang, L. F. Qiao, Z. Q. Jiao, H. Tang, and X. M. Jin, *Optica* **2019**, 6, 2334.

[42] J. Noh, T. Schuster, T. Iadecola, S. Huang, M. Wang, K. P. Chen, C. Chamon, and M. C. Rechtsman, *Nat. Phys*. **2020**, 16, 989.

[43] A. J. Menssen, J. Guan, D. Felce, M. J. Booth, and I. A. Walmsley, *Phys. Rev. Lett.* **2020**, 125, 117401.

[44] D. Tan, Z. Wang, B. Xu, and J. Qiu, *Advanced Photonics* **2021**, 3, 024002.

[45] W. Yan, D. Song, S. Xia, J. Xie, L. Tang, J. Xu, and Z. Chen, *ACS Photonics* **2021**, 8,3308.

[46] C. W. Peterson, T. Li, W. A. Benalcazar, T. L. Hughes, and G. Bahl, *Science* **2020**, 368, 1114.

[47] C. W. Peterson, T. Li, W. Jiang, T. L. Hughes, and G. Bahl, *Nature* **2021**, 589, 376.

[48] Y. Liu, S. Leung, F. F. Li, Z. K. Lin, X. Tao, Y. Poo, and J. H. Jiang, *Nature* **2021**, 589, 381.

[49] X. Ni, M. A. Gorlach, A. Alu, and A. B. Khanikaev, *New J. Phys.* 2017, 19, 055002.

[50] G. G. Pyrialakos, N. Schmitt, N. S. Nye, M. Heinrich, N. V. Kantartzis, A. Szameit and D. N. Christodoulides, *Nat. Commun*. **2020**, 11, 2074.

[51] L. J. Maczewsky, M. Heinrich, M. Kremer, S. K. Ivanov, M. Ehrhardt, F. Martinez, Y. V. Kartashov, V. V. Konotop, L. Torner, D. Bauer, and A. Szameit, *Science* **2020**, 370, 701.

[52] S. Xia, D. Jukić, N. Wang, D. Smirnova, L. Smirnov, L. Tang, D. Song, A. Szameit, D. Leykam, J. Xu, Z. Chen, and H. Buljan, *Light Sci. Appl.* **2020**, 9, 147.

[53] S. Mukherjee, and M. C. Rechtsman, *Science* **2020**, 368, 856.

[54] S. Mukherjee, and M. C. Rechtsman, *Phys. Rev. X* **2021**, 11, 041057.

[55] S. S. Kruk, W. Gao, D. Choi, T. Zentgraf, S. Zhang, and Y. Kivshar, *Nano. Lett.* **2021**, 21, 4592.

[56] M. S. Kirsch, Y. Zhang, M. Kremer, L. J. Maczewsky, S. K. Ivanov, Y. V. Kartashov, L. Torner, D. Bauer, A. Szameit, and M. Heinrich, *Nat. Phys.* **2021**, 17, 995.

[57] Z. Hu, D. Bongiovanni, D. Jukic, E. Jajtic, S. Xia, D. Song, J. Xu, R. Morandotti, H. Buljan, Z. Chen, *Light Sci. Appl.* **2021**, 10, 164.

Table of Contents

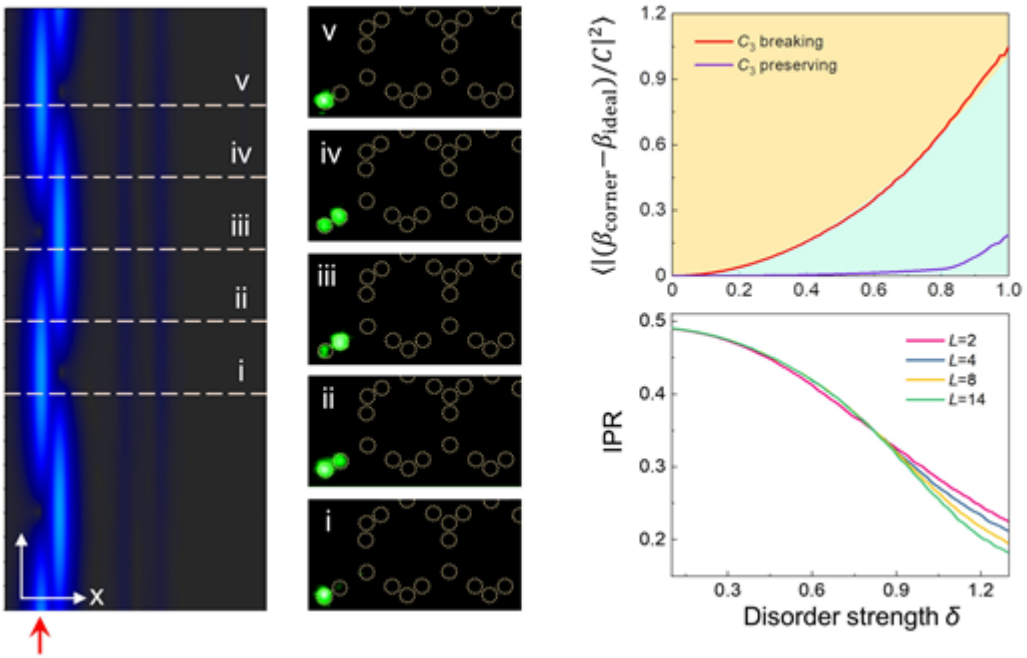

A 2D photonic square-root HOTIs is realized in photonic waveguide arrays written in glass using femtosecond laser direct-write techniques. In addition to the spectral measurement, we analyze a fractional corner anomaly for revealing the higher-order topology, and explored the confinement and robustness of the corner states. These findings offer a feasible strategy for controlling symmetry-protected localized states, and pave a way toward potential applications in photonic devices.